Degradation of Fan Performance in Cooling Electronics: Experimental Investigation and Evaluating Numerical Techniques

Yaman. M. Manaserh[1], Mohammad. I. Tradat[1], Cong Hiep Hoang[1], Bahgat G. Sammakia[1], Alfonso Ortega[2], Kourosh Nemati[3], Mark J. Seymour[3]
[1]Departments of Mechanical Engineering, ES2 Center, Binghamton University-SUNY, NY, USA
[2]Departments of Mechanical Engineering, ES2 Center, Villanova University, PE, USA
[3]Future Facilities, London, UK and NY, USA
E-mail: yyaseen1@binghamton.edu

Abstract

This study reports on the essential forced air-cooled electronics issue of fan performance deterioration caused by the presence of obstructions inside Information Technology Equipment (ITE). Fan performance was characterized based on the fan's static pressure and flowrate. Three different experimental techniques (flow test chamber, pressure probe, and pressure taps) were used to measure the fan static pressure at different locations. Moreover, Computational Fluid Dynamics (CFD) models were built considering different fan working environments. Multi Reference Frame (MRF) and Lumped Fan (LF) model CFD techniques were employed. The experimental results were used to evaluate the modeling techniques whilst implemented in different working environments and to better understand how fans react to blockages inside ITE. Experiments showed that compared to the Free Environment (FE) readings, placing the fan inside a specific ITE reduced the flowrate delivered by the fan by 57.2% and decreased static pressure by 76.3%, which affects the thermal performance of the ITE cooling system. Moreover, comparing numerical results with the experimental ones showed that the MRF approach predicted the flowrate delivered by the fan with a relative error of 3.9%, while the LF approach overestimated the flowrate by 70.3%. The results and conclusions reported in this work can be expanded to cover many other applications in which fans are operating inside enclosed environments and surrounded by many obstructions.

Keywords: thermal management; electronics cooling; IT-equipment; axial flow fans; CFD; multiple reference frame.

1. Introduction

Enhancement of thermal management is becoming a bottleneck challenge that restricts the further development of many sectors such as the lithium-ion batteries industry [1-3] and the electronics industry [4-9]. Developing technology trends and increasing demand for online services have prompted rapid growth in data management, storing, and processing, which in turn has increased the waste heat dissipated by ITE [10]. These facts have prompted researchers to investigate potential solutions and reliability concerns regarding electronics thermal management. A. Taheri et al. [11] proposed a new design of a liquid-cooled heat sink to enhance the thermal performance of available cooling modules in the electronics market. B. Kanargi et al. [12] performed a numerical and experimental investigation on an air-cooled oblique- finned heat sink considering two oblique angles which are 30° and 45°. H. Saber et al. [13] performed a performance optimization study to minimize the non-uniformity of the temperature distribution in the computer chip and its power requirements. This was done by considering cascaded and non-cascaded thermoelectric devices for cooling computer chips. T. Yeom et al. [14] investigated the enhancement of parallel channels air-cooled heat sink using a piezoelectric synthetic jet array for electronics cooling. M. Yang et al. [15] conducted an- experimental study on single-phase hybrid microchannel liquid-cooled chips. Their study introduces a novel hybrid microchannel heat sink combining manifold with secondary oblique channels. These studies mainly focused on the heat sink design whether it was air cooled or liquid cooled-

Nomenclature		$\bar{v}$	Average velocity ($m\ s^{-1}$)
CE	Chassis environment	$\vec{v}$	Absolute velocity ($m\ s^{-1}$)
CFD	Computational fluid Dynamics	$\vec{v}_r$	Relative velocity ($m\ s^{-1}$)
$\vec{F}$	Body forces ($kg\ m\ s^{-2}$)	y	Distance to the wall (m)
FE	Free environment	y^+	Dimensionless parameter
ITE	Information technology equipment	ε	Rate of turbulent kinetic energy dissipation ($m^2 s^{-3}$)
k	Turbulent kinetic energy ($m^2 s^{-2}$)	ν	Kinematic viscosity
LF	Lumped fan	ρ	Fluid density ($kg\ m^{-3}$)
MRF	Multiple reference frame	$\bar{\bar{\tau}}$	Viscous stress tensor ($kg\ m^{-1}\ s^{-2}$)
P	Pressure ($kg\ m^{-1}\ s^{-2}$)	$\vec{\omega}$	Angular velocity (s^{-1})
$\dot{Q}$	Volumetric flowrate ($m^3 s^{-1}$)	**Subscripts**	
SE	Server environments	c	Converted
$\vec{u}$	Velocity vector ($m\ s^{-1}$)	w	Wall
$\vec{u}_r$	Whirl velocity ($m\ s^{-1}$)	τ	Friction

-heat sinks. However, heat sinks design is not the only topic that attracted the researchers' attention in the electronics cooling research field.

As fans continue to play an integral role in electronics cooling, researchers extensively investigated many aspects related to implementing fans in the electronics thermal management applications, such as fan geometry, fan characterization, and improving convective heat transfer. Their investigations considered different types of fans namely, axial fans [16, 17], piezoelectric fans [18, 19], and centrifugal fans [19, 20]. Generally, ITEs tend to be physically dense environments. Fans often operate surrounded by multiple objects, which form obstructions that can degrade the fan's performance. Some of the obstructions' effects on fan performance have been previously studied. S.Lin and C.Chou [21] experimentally investigated the blockage effect on the performance and noise characteristics of axial-flow fans mounted on the heat sink assembly. Their results showed that the decrease in flowrate was insignificant while the static-pressure loss was dramatic. In another study [22], the authors examined the blockage effect on the radial fans and presented a comparison showing how axial and radial fans each react to blockage. They concluded that radial fans are more suitable for environments with high resistance.

S. Nakamura et al. [23] carried out a numerical and experimental study that discussed the influence of an upstream obstacle on the flow characteristics of axial-flow fans. It was concluded that the propagating velocity ratio depends on the non-dimensional diameter (blockage diameter to fan diameter ratio). The authors' follow-up study [24] compared the effects of upstream and downstream blockages on the fan's performance, the results of which showed that they have different consequences. At a small distance, the pressure coefficient decreased with an upstream blockage but increased with a downstream blockage. A. Al-Salaymeh and O.Badran [25] performed an experiment to identify the influence of installing various types of grilles at the fan's inlet and outlet. Their experiment showed that using some types of grilles improved fan performance. However, all of these studies experiment were performed in FE.

Regarding the enclosure environment, T. Fukue et al. [26] used a perforated plate to imitate ITE components in order to investigate the effect of closing part of the perforated plate on the fan performance. In another work, they studied pressure drop in an enclosure with different obstructions and investigated its relationship with the (P-$\dot{Q}$) curve. [27] Their results revealed that the intersection point of a (P-$\dot{Q}$) curve and a flow resistance curve might not predict the actual flowrate when fans are operating inside an enclosure. In a later study, the pressure-drop around the fan in a high-density packaging ITE was evaluated by comparing the conventional pressure drop database with the experimental measurements. [28] Their evaluation aimed to predict the flowrate of a fan in ITE.

When it comes to cooling electronic enclosures CFD modeling, LF modeling, also known as the Abstract fan model, is the most popular approach. LF is a simplified model that calculates the flow through fans using the continuity equation and the fan performance curve, hence a pressure jump is defined between the fan inlet and outlet [29]. R. Boukhanouf and A. Haddad [30] used the LF model for conducting a numerical study on cooling electronics enclosure used in telecommunication systems. P. Nasirabadi et al. [31] performed a transient CFD analysis for thermal field long time prediction inside an electronics enclosure using the LF model. Z. Song [32] utilized the LF model in examining the fan-assisted cooling in open and closed data centers. H. Alissa et al. [33] implemented the LF model in characterizing the reliability of an open compute storage system from the server to aisle levels.

One of the major shortcomings for the LF approach is that it cannot predict the velocity profile of the flow leaving the fan. Instead, it assumes that the flow leaving the fan is unrealistically uniform. One proposed solution to solve the uniform flow assumption is to introduce swirl to the flow field by coupling the LF model with a model that assumes that a certain portion of the total kinetic energy (i.e. 5%) at the fan intake is responsible for generating the swirl component [34]. However, this solution is also not realistic, and it does not represent the actual fan flow field as it just transforms the uniform straight flow into a swirling flow based on assumptions made by the user. Further discussion on this matter is presented in following sections.

As mentioned previously, fans face the difficult issue of cooling ITE with a continuously increasing demand. Therefore, to help solve this issue, improving the accuracy with which fan cooling performance is predicted is a priority. Previous research proposed using the MRF approach as an alternative to the LF approach. [29, 34] MRF, also known as the frozen rotor model, was first presented in 1994, [35] to predict the flow fields induced by impellers in mixing vessels. The MRF approach was widely employed in characterizing fans, Y. Lee and H. Lim [36] presented a study aimed at developing an optimized design of a centrifugal blower by changing the shape of its internal components such as the external cases and the rotating fan ribs. X. Ye et al. [37] numerically investigated the effect of five blade tip patterns on the performance and acoustics of a twin-stage variable-pitch axial fan. Zhang et al. [38] examined the influence of abnormal deflection of two adjacent moving blades in an axial fan by comparing the flow field in the rotor, static and dynamic characteristics of normal blades, and four abnormal blade combinations under the rotating stall. Another study [39] performed CFD and computational aeroacoustics analyses to investigate the acoustic performance of unevenly spaced blades in a centrifugal fan with forward curved blades. The results of these studies have confirmed the reliability and the applicability of the MRF approach. Thus, it can be recognized as a potential substitution for the LF approach in modeling electronics enclosures.

Recently, researchers started to implement the MRF approach while modeling fans for ITE cooling applications. Studies [29] and [40] provided a validation of the MRF fan model by comparing the MRF and the LF models with the vendor flow curve for an electronic enclosure fan. The comparison of flow characteristics showed that the MRF fan model was more representative of the fan prototype than the LF model was. In the following works [41] and [34], the thermal field computed by various fan modeling techniques including MRF for air-cooled enclosures was examined. The results showed that the temperature values obtained from the LF model and the MRF technique differ considerably. Furthermore, the MRF was implemented for improving the accuracy of numerical analysis of a thermal management system for a small data center [42].

This study aims to clarify the obstructions' effect on fan performance inside real ITE. Moreover, it focuses on assessing the accuracy of both the LF and MRF approaches in representing the fan performance inside high resistive ITEs. The fan performance was assessed based on the static pressure and flowrate. The experimental setup was designed to consider pressure measurements at different locations using three different pressure measurement techniques: pressure probe, pressure taps, and test chamber. The fan was tested experimentally in three different environments: FE, empty server Chassis Environment (CE), and the full Server Environment (SE). CFD models were developed to replicate these environments and were solved using LF and MRF approaches. The results of the two CFD approaches and the experimental results were compared. After that, the fan's flow field was investigated thoroughly at different locations within the system. What distinguishes this study is that it investigates the fan performance inside its actual working environment instead of testing it in FEs. Additionally, this work considers how fan performance is affected by actual blockages rather than disks that imitate blockages. The results of this study show that some blockages have a significant effect on fan performance, depending on the size of the blockage, distance from the fan, and the working environment. This work may also provide researchers and industry engineers with a general idea of the margin of error present when modeling fans inside high-density ITEs and the best technique to use in their models. Finally, since fans are used for cooling and ventilation purposes in many other applications that have a similar working environment to the ITEs, the conclusions of this study are not limited to electronics cooling and it can be beneficial in such applications as well for instance, automotive industry and electrical devices (power supplies, projectors, etc.).

2. Experimental setup

2.1. Testing environments

The fan was tested in three different environments. The reason behind this is to show how the fan reacts to different operating environments. Additionally, it can give an overall estimation of the error that could result from using the fan performance curve to predict fan performance in such environments.

The first testing environment, which is referred to as FE, is most similar to the environment that vendors use to conduct their fans performance curves in which the fans are tested according to a set of standards. One of the most widely adopted standards in the fan industry is "ANSI/AMCA Standard 210-16/ ASHRAE Standard 51-16: Laboratory Methods of Testing Fans for Certified Aerodynamic Performance Rating" [43]. By testing the fan in this environment, a flow curve was attained which was used as a reference for fan performance when there are no blockages.

In the second testing environment, which is called the CE, the fan was installed inside an empty server chassis (no components) and this chassis was connected to the flow chamber. By testing the fan in this environment, the enclosure effect on the fan behavior was investigated.

The third testing environment, which is referred to as SE, is about testing the fan inside a server chassis containing all of the chassis components as blockages. By testing the fan in this environment, the researchers aim to clarify how the fan performs inside actual ITE and obtain a general idea of fan performance degradation inside actual ITE. However, given that different ITE configurations will produce different fan behaviors, the results of this study cannot be generalized to all fan-ITE configurations. The three testing environments and the 3D views of both CE and SE are shown in Fig.1.

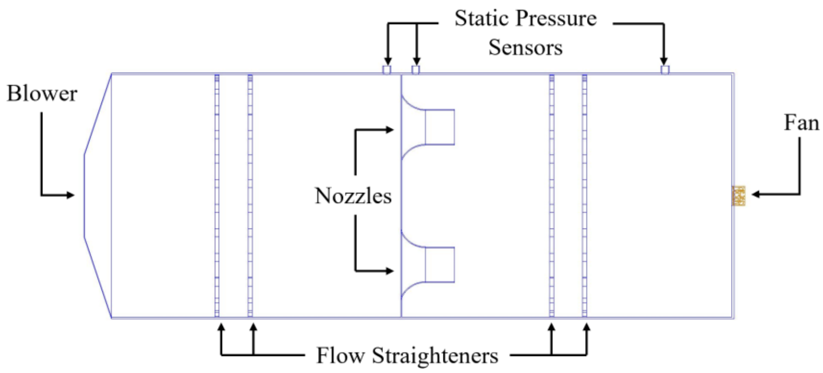
Static Pressure Sensors
Blower
Fan
Nozzles
Flow Straighteners

(a) FE

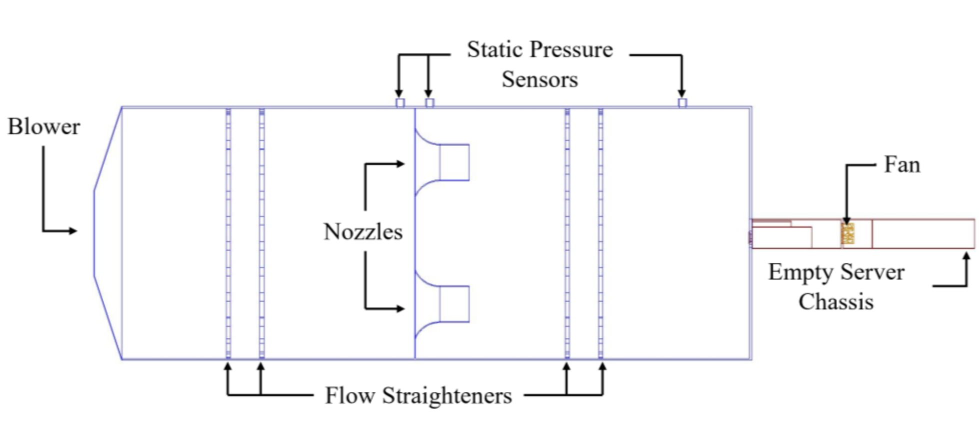
Static Pressure Sensors
Blower
Fan
Nozzles
Empty Server Chassis
Flow Straighteners

(b) CE

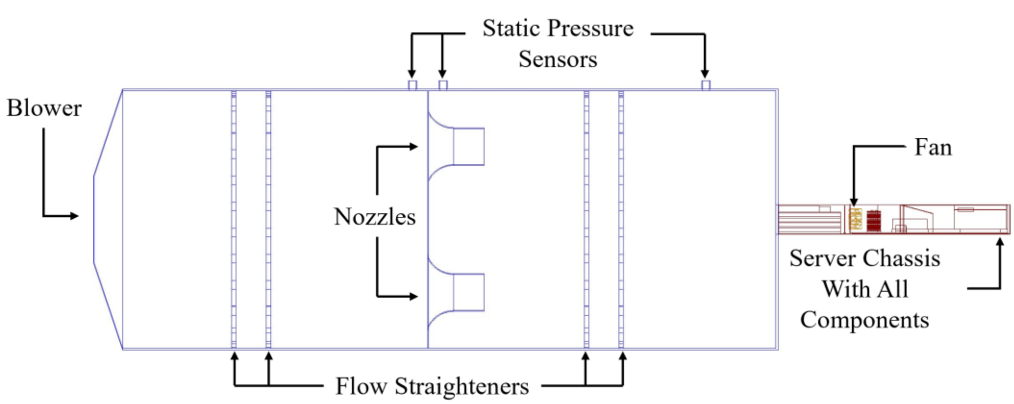
Static Pressure Sensors
Blower
Fan
Nozzles
Server Chassis With All Components
Flow Straighteners

(c) SE

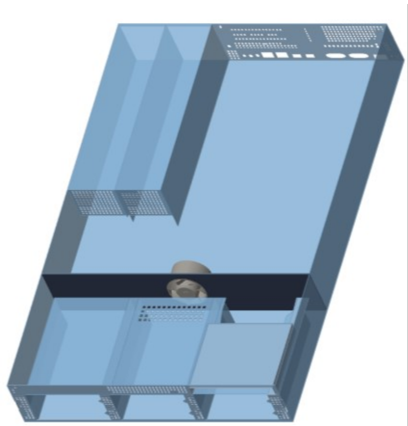

(d) 3D view of CE

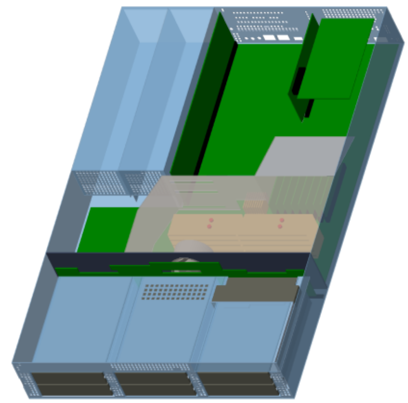

(e) 3D view of SE

Fig. 1. Schematic diagram and 3D views of different working environments.

2.2. Measurements techniques

The fan flowrate was reported based on the differential pressure across the flow chamber nozzles. Simultaneously, the static pressure was measured inside the chamber near the fan inlet. For both CE and SE, the static pressure sensor measurements from the chamber did not represent the actual static pressure generated by the fan, because they were taken far away from it (distance between fan and test chamber sensor). Therefore, two additional methods of pressure measurement were introduced to obtain more accurate pressure measurements.

The second technique was a static pressure probe, which was used to measure the static pressure inside the server. The first step in this process was replacing the server cover with a plexiglass sheet. Next, a slot was drilled into the sheet at the fan inlet location for a probe to be inserted through. A linear motion mechanism was then used to drive the pressure probe along the slot to take measurements at different locations. To avoid interrupting the flow, a small diameter probe was used, the details of which are presented in Fig. 2 (a) and (c). One drawback of this technique is that it has a space limitation, so if the ITE is spaced too densely, then using this technique is not possible.

The third technique was pressure taps, which were used to measure the static pressure at the enclosure's cover near the fan inlet. Pressure taps were drilled into a half-inch plexiglass sheet, which was used to replace the cover of the enclosure. The geometry of the pressure taps was obtained from [44]. The pressure taps hole has two diameters, one to fit the stainless steel tubulation and the other one is to take measurements. A plastic tube was used to connect the stainless steel tubulation to the pressure transducer to take pressure measurements through the taps. An advantage of this technique is that it is not limited by the available space. However, its disadvantage is that it cannot provide detailed pressure measurements from inside the enclosure. Fig. 2 (b) and (d) show the third pressure measurement technique in detail.

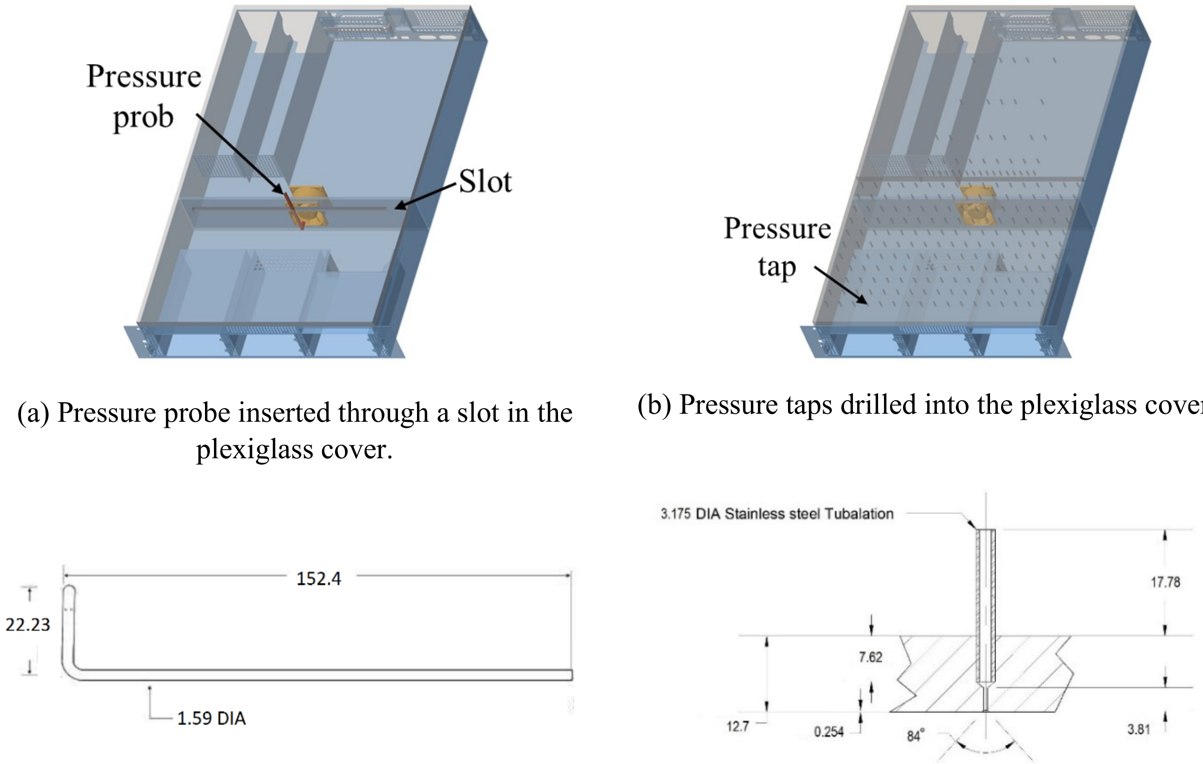

(a) Pressure probe inserted through a slot in the plexiglass cover.

(b) Pressure taps drilled into the plexiglass cover.

(c) Dimensions of the static pressure probe

(d) Details of the static pressure tap

Fig. 2. Static pressure measuring techniques.

Before running the test, it was important to obtain the time required by the fan to reach steady- state. The fan was turned on for 15 seconds which is the time assumed to reach steady state. Then, measurements were taken every 30 seconds for 5 minutes. The average and the standard deviation were calculated for these pressure measurements. Thereafter, the average was compared with two readings taken at 15 and 20 minutes. In order to conduct a thorough investigation, the pressure readings were taken at different fan flowrate. Fan flowrate was controlled using a variable openness gate. From Table 1, it can be inferred that 15 seconds is sufficient time to ensure the steady state conditions. It should be noted that these measurements were taken in an arbitrary environment that is not discussed in this paper for the sake of simplicity and consistency of the manuscript. This environment is similar to the CE but with some blockages installed inside it. This explains the small difference between these measurements and the SE ones reported in following sections. However, the time for reaching steady state is observed to be the same for all environments.

2.3. Instrumentation and experiment procedure

In this experimental setup, a flow test chamber was utilized to control the flowrate and to measure the static pressure near the chamber outlet. In CE and SE, the additional static pressure readings collected through the pressure taps and the pressure probe were done using a pressure transducer and a DAQ (data acquisition) system. For the ITE configuration in SE, the pressure probes could not be used due to limited space, hence pressure measurements were collected using the pressure taps. In addition, a DC source and a tachometer were used to control the fan speed. The fan speed was maintained constant by adjusting the power supply output voltage [21, 27]. In all experiments conducted in this study, the fan rotational speed was set to 12000

RPM, which equals to the vendor's testing speed. This speed was adopted to keep consistency in our results and to execute a fair comparison between our results and the vendor's ones.

Even if the fan power is an essential factor for characterizing fans, the fan's power was not recorded along the experiment. This is attributed to the fact that this study aims to characterize the fan's performance in cooling electronics rather than characterizing the fan itself. However, general observation of the fan power during the experiment revealed that the fan consumes more power in highly resistive environment (SE) compared to the FE, although tests were conducted at an equal rotational speed. More in-depth discussion on the fan power variation when it is being blocked can be found in [23, 24].

Table 1
Static pressure reading variation with time.

Time	$\dot{Q}$=0 ($m^3.s^{-1}$)		$\dot{Q}$=16 × 10^{-3} ($m^3.s^{-1}$)		$\dot{Q}$=24.07 × 10^{-3} ($m^3.s^{-1}$)	
	Pressure P (Pa)	Standard deviation	Pressure P (Pa)	Standard deviation	Pressure P (Pa)	Standard deviation
5 mins (average)	225.18	1.14	110.78	1.14	46.36	1.319
15 mins	225.95	-	110.73	-	45.79	-
20 mins	225.45	-	111.23	-	46.28	-

To yield reliable measurements while characterizing the fan performance, all experimental work was conducted using a test chamber that was designed in accordance with AMCA 210-99 standards [45]. An appropriate size nozzle was installed in the chamber to capture the whole fan performance curve. Moreover, a non-contact tachometer (Uni-t ut372) was used to avoid interfering with the fan performance. The merit of this tachometer is that it has a high accuracy (0.04% ±2dgt) over a considerably wide measurements range (0~99999 RPM).

Besides the test chamber pressure sensor, a pressure transducer with relatively low differential pressure measurement range (1333 Pa) was used to take measurements through the pressure taps and the pressure probe, it was chosen to consider that the static pressure for a typical fan used electronics cooling is small. This pressure transducer and the chamber pressure sensors were calibrated prior to running the experiments. This was done by comparing their measurements against a variable-pressure reference device. Hence, by changing the reference device pressure and collecting the data from our sensors, a correlation between the actual pressure and the sensor measurement was derived which were used to improve the sensors measurements accuracy. Instrumentation models and specifications are summarized in Table 2.

The experiment in the three environments was conducted according to airflow test chamber manual which is derived from AMCA's fan testing standards [45], the experimental procedure can be summarized as follows (The reader is referred to Fig. 1 in locating the corresponding components when describing the experiment procedure): in the FE, the pressure sensors were calibrated to measure zero pressure differential with respect to the room. Next, the fan was directly connected to the flow test chamber, and the fan speed was set to equal to the vendor's testing speed. After that, the fan performance curve was derived by varying the fan flow rate between zero and the free delivery point while recording the fan's static pressure readings. The air was initially blocked from entering the fan by the test chamber gate to record the highest pressure that can be generated by the fan, then the gate was opened gradually, and an external blower was used to control the flow rate to take deferent measurements until the free delivery point is achieved, at which the static pressure at the fan inlet equals to zero. Next, the flowrate at different points was reported using the pressure difference across the nozzle and the vendor's pressure differential- flowrate charts for the used specific nozzle. Finally, these different flow delivery readings were used along with corresponding static pressure measurements to plot the fan performance curve. Regarding the CE and the SE, a similar procedure was followed except that the fan is installed in a different environment while pressure measurements are simultaneously recorded through the flow test chamber sensor and the pressure probe or the pressure taps. Also, in these two environments, the flow is restricted to pass around the fan by installing an obstruction as shown in Fig.1 (d) and (e).

Table 2

Details of instrumentation used in the experimental setup.

Instrument	Specifications
Airflow test chamber	Designed in accordance with AMCA 210-99 standards.
DC source	KEYSIGHT E3634A
Tachometer	Uni-t ut372 (accuracy : 0.04% ±2dgt)
Pressure transducer	MKS 698A (accuracy: 0.08% of the reading)
DAQ	National Instruments cDAQ-9171

3. Numerical modeling

3.1. Simulation method

Simulations were carried out using the commercial CFD package of Fluent. The following assumptions were made while running the simulations: heat transfer between solid bodies and the air is negligible, air is incompressible and has constant properties, and the impacts of wall roughness and gravity are negligible. Based on these assumptions, the energy equation was disregarded. The boundary conditions of the inlet and outlet were set as pressure-based conditions. The value of the inlet pressure boundary was adjusted to measure the different points of the fan performance (P-$\dot{Q}$) curve while keeping constant zero pressure at the outlet.

Two CFD approaches were deployed to model the fan in different environments. The first approach is the LF model. Due to the simplicity of this model and the fact that it is computationally inexpensive, it is the most widely adopted fan modeling approach in the electronics cooling industry. In this approach, fan geometry is replaced by a 3D solid body or a 2D surface replicating the fan dimensions. Between the fan's upstream and the downstream faces, the fan flowrate is calculated using the continuity equation and a pressure jump function without solving the Navier-Stokes equations. The pressure jump function is typically derived from the vendor's fan performance curve. In this study, the pressure-rise (ΔP) across the fan was specified as a function of average-velocity ($\bar{v}$) normal to the fan. The average velocity through the fan was calculated by utilizing the vendor fan performance (P-$\dot{Q}$) curve as illustrated in Table 3. However, some CFD packages are more robust as the fan performance curve is directly imported to the code, and it will automatically generate the pressure jump function and define it for the fan.

According to the definition of LF approach, the flow leaving the fan is defined to be uniformly distributed and normal to the downstream fan face. The swirl function, which is used to transform the straight flow into swirling flow, can be incorporated into the solution in many ways such as defining Swirl Number or Peak Impeller Efficiency, depending on the CFD package. Basically, all of these methods of defining the swirl function are generating the swirl by imposing unrealistic tangential and radial velocity fields on the downstream fan surface. Thus, they are all expected to fail in predicting the actual fan flow field which results from the interaction between air and the fan components (blades, outlet guide vanes, etc.).

On the way how the LF approach deals with the different fan speeds, the LF model utilizes the fan affinity laws [46] to calculate the fan flowrate $\frac{Q_1}{Q_2} = \frac{\omega_1}{\omega_2}$, and static pressure $\frac{P_1}{P_2} = \left(\frac{\omega_1}{\omega_2}\right)^3$ from the fan performance curves. Thus, if the fan is speed is different from the vendor's rated speed (the speed adopted by the vendor while conducting their fan performance curve), the fan performance curve will be automatically modified according to the fan affinity laws.

Table 3

Vendor's fan performance (P-$\dot{Q}$) curve and average velocity through the fan.

Pressure P (Pa)	Flowrate $\dot{Q}$ $(m^3.s^{-1} \times 10^{-3})$	Average velocity $\bar{v}$ $(m\,.s^{-1})$
530.03	0	0
403.12	6.04	3.8
261.28	14.11	8.88
248.84	15	9.44
241.37	15.88	9.99
233.91	17.03	10.71
231.42	18	11.32
228.93	19.06	11.99
226.94	20.11	12.65
221.47	21.17	13.32
214	22.23	13.99
201.56	23.56	14.82
171.7	25.41	15.99
129.4	27.72	17.44
57.23	30.73	19.33
0	32.86	20.67

Based on the vendor flow curve and the corresponding average velocity through the fan, a polynomial regression was performed to derive the fan's pressure rise function. The fifth-order polynomial that describes the pressure jump across the fan based on the average velocity is given by Eq. 4. The goodness of fit of the regression was tested by calculating the R-squared which was found to be equal to 99.96%.

$$\Delta P = 0.0017\bar{v}^5 - 0.0966\bar{v}^4 + 1.8465\bar{v}^3 - 12.679\bar{v}^2 - 6.7324\bar{v} + 529.92 \quad (1)$$

The second approach was the MRF approach, the steady state MRF approach is used to model rotating parts in CFD using its 3D geometry. Since that the MRF approach is a steady state method, it requires significantly lower amount of computational resources compared with the other 3D fan modeling approaches that include the rotor geometry such as sliding mesh [47]. However, compared with the LF model, the special grid treatment that needs to be done on the fan body in the MRF approach makes it more computationally expensive than the LF approach. A detailed comparison between the number of grids required by each approach to assure convergence is presented in a later section.

The MRF is modeling rotating parts by separating the fluid domain in the CFD model into rotating regions and non-rotating regions. In the rotating region, the governing equations are transformed into a rotating frame. By doing so, the centripetal and Coriolis acceleration are incorporated into the governing equation [48].

Thereby, in the rotating region, the fluid is moving around fixed geometry (in our case fixed geometry is the fan blades) instead of rotating the body through the non-rotating air. This is similar to taking a snapshot and observing the instantaneous fluid streamlines around the rotating body in this certain position. This is why this approach is also called the "frozen rotor model". However, the following geometrical conditions must be met to apply the MRF approach first, the rotating region must be axisymmetric second, the rotating region must have an axis of rotation that is concentric with the rotating parts finally, all the rotating parts must be bounded withing the rotating region also, it is recommended that rotating region extends beyond the rotating parts by a small distance [29].

As mentioned before, the MFR approach considered a coordinate system that steadily rotated with angular velocity $\vec{\omega}$ relative to a stationary (inertial) reference frame. The conservation of mass and momentum equations (equations 2 and 3 respectively) of fluid flow for a steadily rotating frame considering the absolute velocity formulation for the rotating frame can be written as follows [49]:

$$\nabla \cdot \overrightarrow{v_r} = 0 \tag{2}$$

$$\nabla \cdot (\vec{v}_r \vec{v})\rho + \rho(\vec{\omega} \times \vec{v}) = -\nabla p + \nabla \cdot \bar{\bar{\tau}} + \vec{F} \tag{3}$$

Where $\vec{v}$ denotes the absolute velocity and $\vec{v}_r$ represents the relative velocity, $\vec{v}_r = \vec{v} - \vec{u}_r$. Next, $\vec{u}_r = \vec{\omega} \times \vec{r}$ and represents the velocity due to the moving frame (whirl velocity). Then, $\vec{\omega}$ and $\vec{r}$ denote the angular velocity and the position vector, respectively. Lastly, $\bar{\bar{\tau}}$, $\vec{F}$ denote the viscous stress tensor and the body forces, respectively.

According to these equations, the fan rotational speed in the MRF is substituted in the governing equations to calculate the fan flow rate and static pressure in contrast to the LF approach, which substitutes the fan speed in the fan affinity laws. Furthermore, what distinguished this approach from the LF approach is that it considered the actual rotating body and the interaction between the rotating impeller and stationary zones. Therefore, the MRF fan model can predict the fan's flow fields extensively more accurately than the LF approach. Fig. 3 shows the difference in fan shape for the LF and MRF approaches.

After discussing fan modeling techniques, the turbulence model needs to be introduced. The internal flow dynamics of axial flow fans are extremely complex and different vortices are found. [50, 51] Therefore, Reynolds Averaged Navier-Stokes (RANS) was considered. The realizable k-ε turbulence model was selected to simulate the flow field through a coupling with RANS equations. This turbulence model was selected according to the literature which has confirmed the reliability of employing the realizable k-ε turbulence model to solve rotating flow [52-56]. In addition, during conducting the simulation, more than one RANS turbulence models were tested, and the results showed that the realizable k-epsilon turbulence produced the most accurate results where some of these models did not even converge.

(a) MRF (b) LF

Fig. 3. Utilized fan shape in MRF and LF modeling approaches.

The realizable k-ε was coupled with the enhanced wall treatment [57], which is a near-wall modeling method that combines a two-layer model with so-called enhanced wall functions. The exceptional advantage of the enhanced wall treatment is that it is a y^+ insensitive method. For this, y^+ is a dimensionless parameter indicating the wall coordinate, $y^+ = \frac{yu_\tau}{\nu}$, $u_\tau = \sqrt{\tau_w/\rho}$ where y is the distance to the wall, u_τ denotes the friction velocity, and τ_w represents the wall shear stress. Enhanced wall treatment acts as a wall function if the first grid point is in the log-layer. Considering a near-wall mesh that is fine enough to resolve the viscous sublayer, the enhanced wall treatment performs like the traditional two-layer zonal model.

Table 4

CFD models details

Case	Environment	CFD approach
Case 1	FE	LF
Case 2	FE	MRF
Case 3	CE	LF
Case 4	CE	MRF
Case 5	SE	LF
Case 6	SE	MRF

3.2. Fan model

CFD models were built to duplicate the three different environments. For each environment, LF and MRF approaches were employed. Hence, a total of six models were simulated, the details of which are briefed in Table 4. Fig. 4 introduces the 3D fluid domains that were developed based on different testing environments. The red body represents the rotating frame. When the LF approach was used, it was replaced by a cylindrical body as shown in Fig. 3 (b). For SE, the golden heat sink depicted in Fig. 4 (e) was used to investigate flow distribution, which is discussed in a later section.

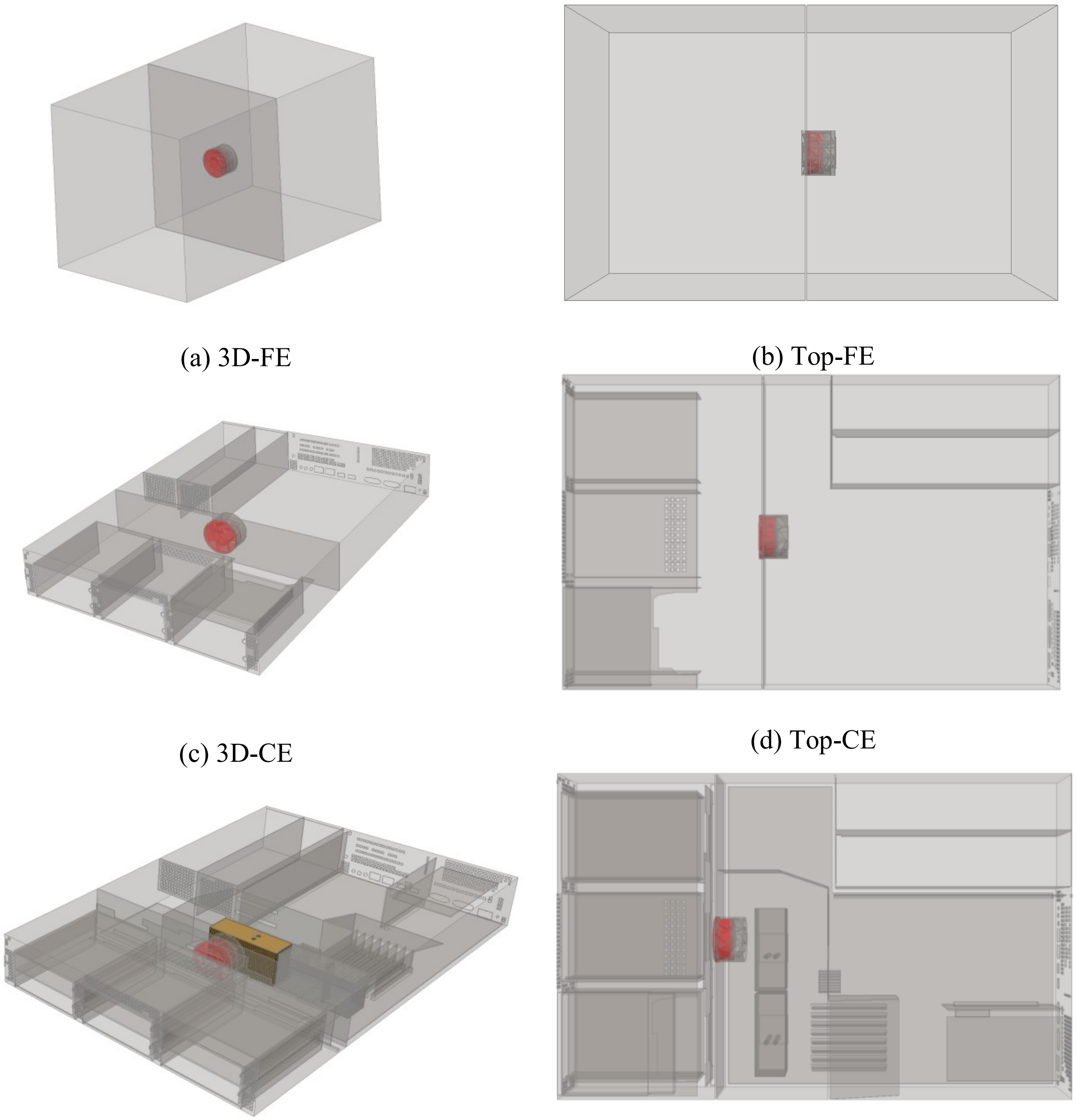

(a) 3D-FE
(b) Top-FE
(c) 3D-CE
(d) Top-CE
(e) 3D-SE
(f) Top-SE

Fig. 4. Perspective 3D and top views for the model fluid domains, replicating the testing environments.

The main structure of the FE model consisted of a pressure inlet, walls upstream of the fan, and pressure outlets downstream of it. For CE and SE, holes at the server inlet were set as pressure inlets, and chassis walls and server components were defined as walls. Lastly, the holes at the back of the server were specified as pressure outlets. Specific structural parameters for the environments, fan, and heat sink are shown in Table 5.

Table 5

Main structural parameters.

Parameter	Value
Environments	
FE model dimensions (mm)	(Height=360, width=360 depth=720)
Server dimensions (mm)	(Height=86.4, width=444, depth=744)
Fan	
Fan hub diameter (mm)	35
Fan inlet bell diameter (mm)	64
Fan tube housing diameter(mm)	57
Fan rotational speed RPM	12000
Number of fan blades	7
Number of outlet guide vanes	5
Heat sink	
Fin dimensions	(Height=0.5, width=110 depth=40)
Number of fins (mm)	30
Pitch (mm)	1.88

3.3. Grid method

The computational domain was first divided into the upstream region, rotating frame or fan region, and downstream region. The grids were created using a polyhedral type element. The advantages of using polyhedral mesh were reported in [58, 59], and it has shown good performance in modeling fans [60-62]. A higher number of elements was considered in the fan region. A sizing function was employed to densify the meshes at the fan walls. Contact sizing was applied at the contact surfaces between different regions to avoid sudden changes in cell size. The element growth rate was 1.1. Maximum skewness was kept under 0.85, where the maximum skewness should be less than 0.97 to assure a high-quality mesh [63]. Fig. 5 illustrates the grid for the fan walls.

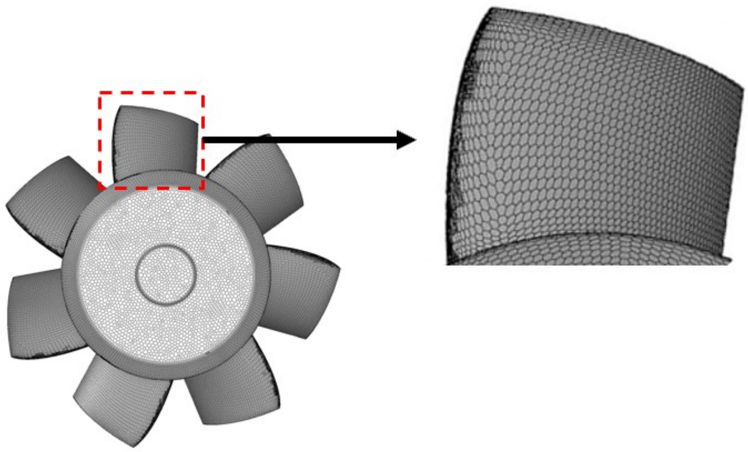

Fig. 5. Mesh of the axial-fan.

Grid sensitivity analyses were conducted to satisfy the requirements of computational accuracy and to eliminate the effect of the grid number on the fan's flowrate and static pressure. The static pressure reading measurement presented an average of nine pressure readings, which were taken at a 3×3 grid $1 \times 10^{-2} m$ away from the fan inlet as shown in Fig. 6. The grid sensitivity analyses were performed using five groups of mesh numbers for each model mentioned in Table 4. The grid number was selected to ensure that variation while increasing the mesh number is kept minimal. For cases 1-6, the mesh number was chosen to be 1.5, 2.2, 1.8, 2.4, 9.4, 10.2 million, respectively. As shown in Fig. 7, MRF (case 2,4, and 6) required a larger number of meshes for fulfilling convergence. However, the difference in terms of the grid number between these two methods was reasonable.

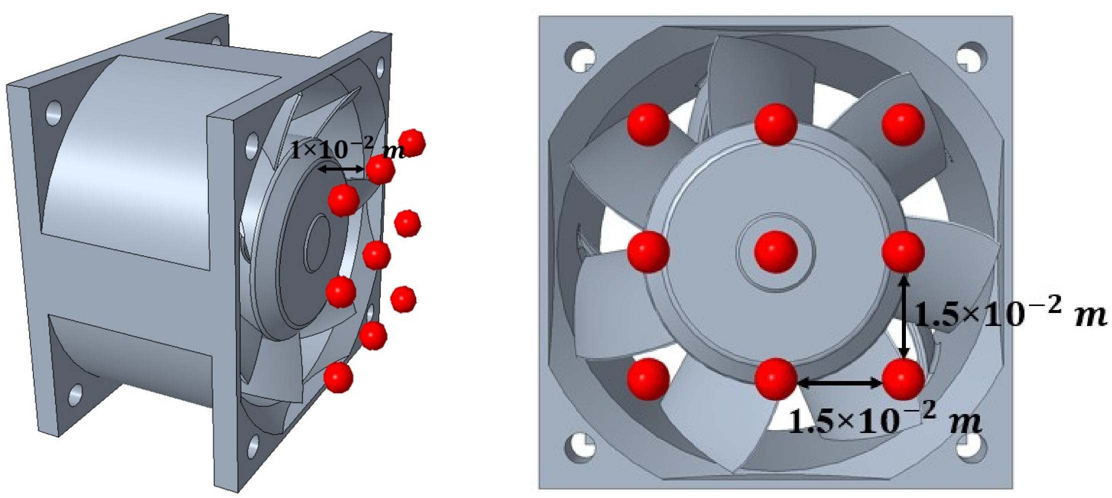

(a) 3D view (b) Front view

Fig. 6. Details of pressure measurement locations.

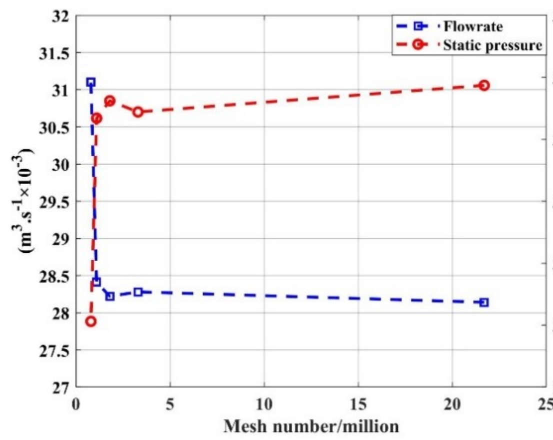

(a) Case 1

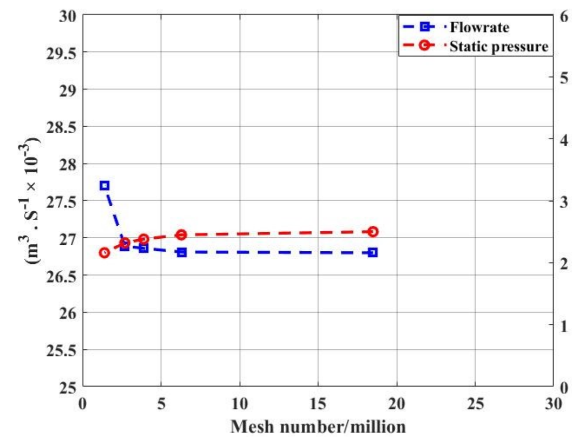

(b) Case 2

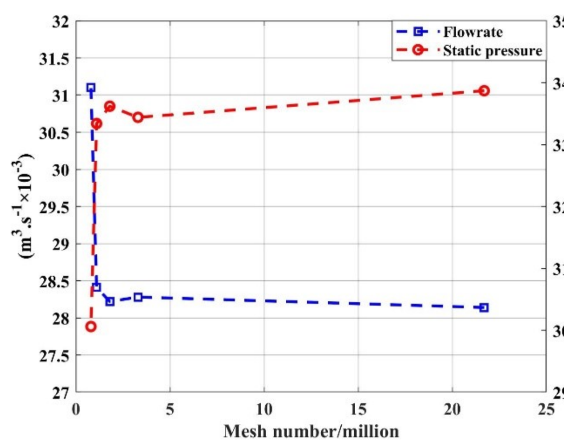

(c) Case 3

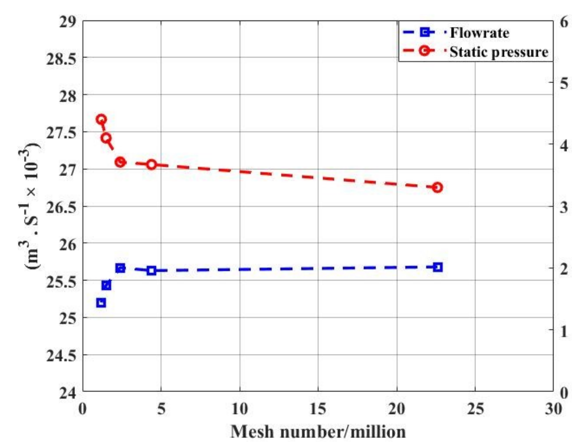

(d) Case 4

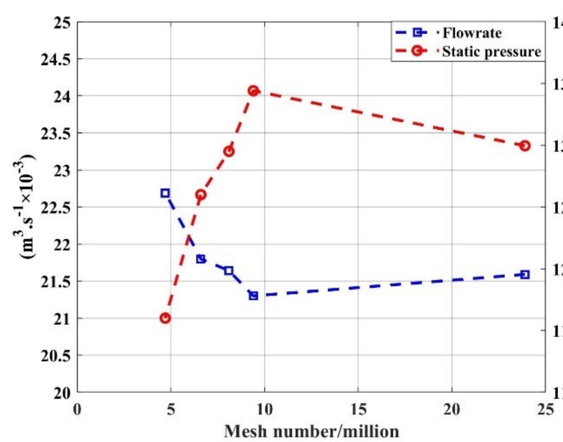

(e) Case 5

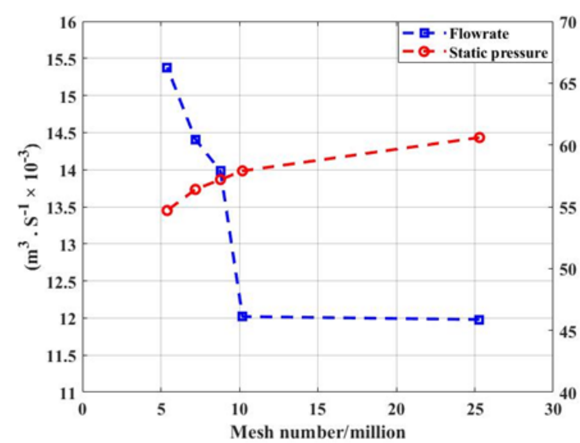

(f) Case 6

Fig. 7. Grid sensitivity analyses.

4. Results and discussion

4.1. Experimental investigation

The first step in evaluating the effect of blockage on fan performance inside a high-density ITE is to obtain a reference for the fan performance. Using the vendor's flow curve might introduce an error to the results because vendors generally test their fans in special flow chambers under preferable operating conditions like room temperature and humidity. This may result in an overpredicted fan performance since these conditions are not necessarily met when the fans perform in a real environment due to changing the air density.

Fans are constant volume machines which means that their flow flowrate is independent of air density. However, the fan's static pressure varies proportionally with air density [64]. The variation in the fan's static pressure due to variation in air density can be calculated using [65]:

$$P_c = P\frac{\rho_c}{\rho} \tag{4}$$

Where P_c, ρ_c are the converted pressure and converted density, respectively. The fan industry rates the fan performance at a standard air inlet density, where the air density is adopted at an inlet temperature of 21°C and at a barometric pressure of 101.32 kPa [65]. In our experiment, the fan was tested at the room temperature (20-22 °C) and at the atmospheric pressure, these conditions are very similar to the fan testing standard. Thus, the difference between experimental air density and the converted one is less than 1%, which means that the experimental results reported in this work do not need to be corrected to "standard air" conditions.

Another reason for the discrepancy between the experimental results and the ones reported by vendors is that fan performance can degrade with time. Hence, for the purposes of this study, a reference performance curve was obtained by testing the fan in the FE using the flow test chamber. Fig. 8 highlights the difference between the vendor flow curve and the actual flow curve. For the FE, the flow delivered by the fan was 11% below what the vendor reported.

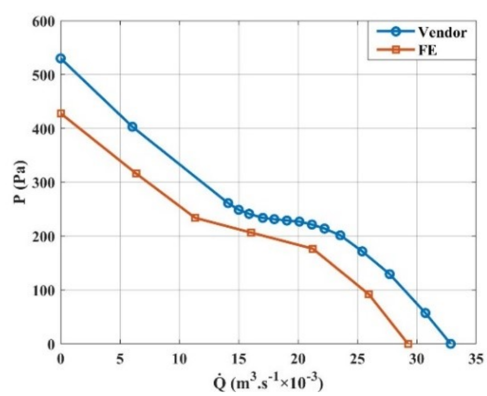

Fig. 8. Vendor's vs actual fan performance curve.

After obtaining the fan performance reference curve, the next step is to investigate the effect of the server chassis on fan performance by testing the fan inside the CE. In this environment, pressure readings were collected by pressure probes, pressure taps, and the test chamber. To form a better understanding of the pressure distribution at the fan inlet, readings were taken on a 3×3 grid using a pressure probe. This is the same method used to take measurements for the numerical models. Fig. 9 presents the pressure readings for three different flowrates at the fan inlet.

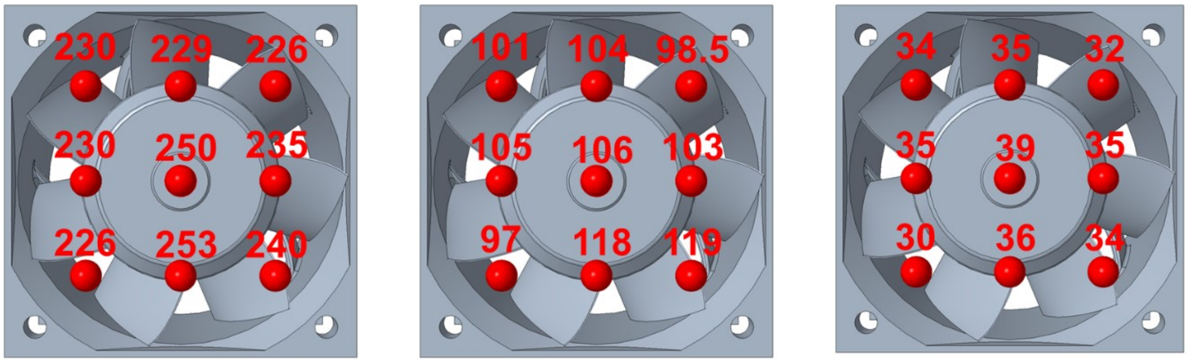

(a) $\dot{Q}$= 0 $(m^3.s^{-1} \times 10^{-3})$ (b) $\dot{Q}$= 16 $(m^3.s^{-1} \times 10^{-3})$ (c) $\dot{Q}$= 24.1 $(m^3.s^{-1} \times 10^{-3})$

Fig. 9. Experimental static pressure measurement at the fan inlet in the CE.

Fig. 9 shows that the pressure readings vary at the fan inlet. This variation occurs due to the heterogeneous configuration of the working environment. However, the pattern of pressure distribution changes with different flowrates.

The comparison of the fan curves obtained using each of the three measuring techniques is illustrated in Fig. 10. It can be inferred from this figure, that the average pressure probe readings showed good agreement with the pressure tap readings. Both techniques provide higher pressure readings than the test chamber due to the presence of the sub-chasses which act as blockages. Furthermore, these obstructions cause a non-zero pressure at the free delivery point (i.e. the maximum flow delivered by the fan). Going from FE to CE, the pressure taps results show a 1.6% drop in the flowrate supplied by the fan and 44.1% drop in the maximum static pressure at the fan inlet This reduction of static pressure represents the enclosure's role in hindering flow into the fan. Hence, ITE enclosure can have a considerable effect on the fan's static pressure.

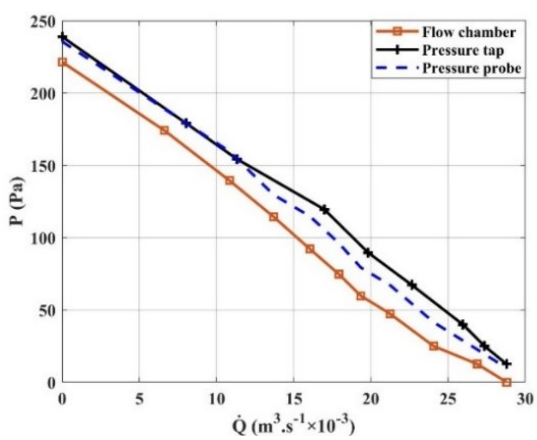

Fig. 10. Fan performance curves in the CE considering various static pressure measuring techniques.

Lastly, the effect of blockages on fan performance was examined in SE. The results are presented in Fig. 11. The figure shows a considerable difference in the pressure readings measured by the pressure taps and the test chamber. At the free delivery point, the flow test chamber reading shows that the static pressure reading equals zero. However, the actual static pressure measurement generated by the fan was 101.3 Pa. This discrepancy in the pressure chamber measurements is attributed to the server components around the fan, which act as obstructions. Based on this, testing the fan inside ITE using a flow test chamber could be misleading in terms of pressure measurements. A summary of the blockages' effect on the maximum fan flowrate and the maximum static pressure at the fan inlet is presented in Table 6, where the maximum static pressure represents the pressure at the fan inlet when the flow delivered by the fan equals zero.

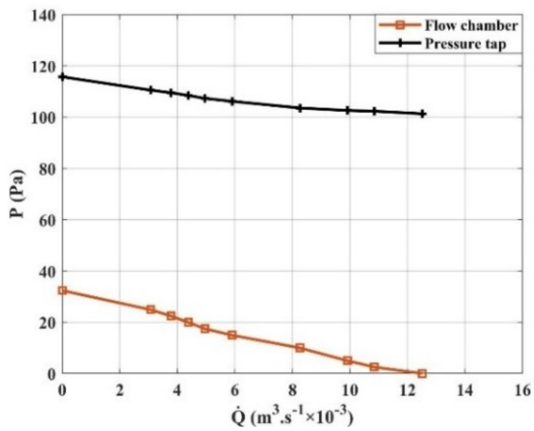

Fig. 11. Fan performance curves based on pressure taps and test chamber static-pressure readings in SE.

Table 6

Operating environment effect on the fan's static pressure and flowrate.

Environment	FE	CE	SE
Pressure measuring technique	Test chamber	Pressure taps	Pressure taps
Static pressure P (Pa)	428 ± 6.22	238.89 ±1.33	101.32 ±1.22
Flowrate $\dot{Q}$ $(m^3.s^{-1} \times 10^{-3})$	29.26 ±0.15	28.79 ±0.14	12.51 ±0.06
Total reduction in maximum pressure (Pa)	-	189.11	326.68
Total reduction in maximum flowrate $(m^3.s^{-1} \times 10^{-3})$	-	0.47	16.75

Table 6 shows that blockages could have a significant effect on both the static pressure and the flowrate delivered by the fan. By comparing the SE with the FE, the fan exhibited a relative reduction by 57.2% and 76.3% in terms of flowrate and static pressure, respectively. This degradation of the fan's performance will vary according to the working environment. Moreover, various fan types and fan shapes may react differently to blockages. Hence, it is vital to consider and investigate how a specific fan reacts to the presence of blockages before using it in ITE. In addition, using the vendor flow curve to predict the fan performance inside ITE may result in a large overestimation of both static pressure and flowrate.

4.2. Analysis of numerical results for fan performance curve

The LF and MRF modeling approaches were tested thoroughly in various working environments. The experimental measurements generated from these working environments were utilized to evaluate the accuracy of these modeling approaches. Table 7 compares the experimental and the CFD results considering the maximum static pressure reading and maximum flowrate.

As can be noted from Table 7, both MRF and LF provide a good estimation of the fan flowrate in the FE where the experimental maximum flowrate was measured to be $29.26 \times 10^{-3}\ m^3.s^{-1}$ and both LF and MRF models predicted 26.18×10^{-3} and $26.89 \times 10^{-3}\ m^3.s^{-1}$, respectively. For maximum static pressure, MRF gives more accurate results than LF, with an error of 15.5% compared to 40% with reference to experimental results, respectively. Note that LF uses the vendor curve, which was previously shown to overestimate the fan flowrate and static pressure, to specify the pressure jump across the fan. Thus, the large mismatch between the LF model and the experiment in the maximum static pressure values can be attributed to this. Fig. 12 shows the vendor fan curve and the experimental flow curves in the CE and the SE.

In the CE, experimental results showed that the fan flowrate slightly reduced and remained 98.39% of that of the FE while the flowrate error decreased to 2% for the LF approach, and increased to 10.8% for the MRF approach. Moreover, it can be noted from the experimental results, that the fan experienced a steep decrease in static pressure. This decrease was not captured by either of the modeling approaches, in fact, the error dramatically increased from 174.19 and 70.45 (Pa) to 382.66 and 246.85 (Pa) for the LF and the MRF models compared with the FE, respectively.

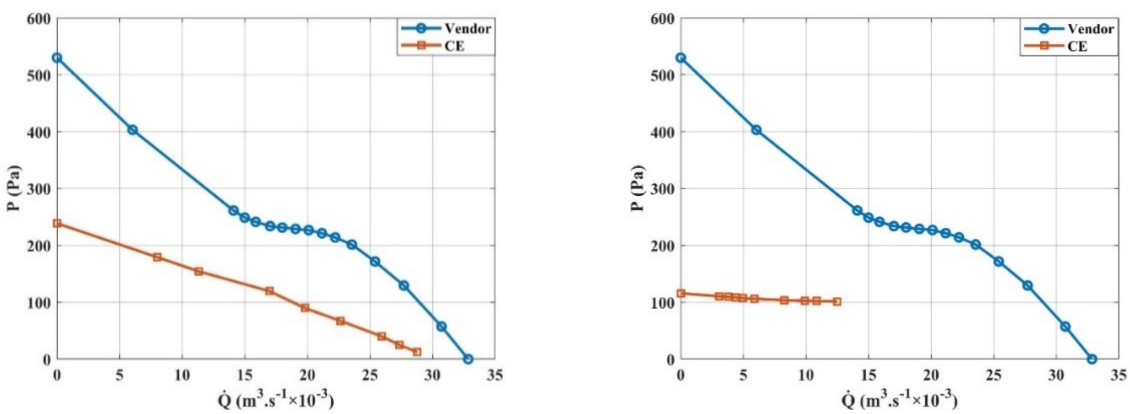

(a) CE (b) SE

Fig. 12. Vendor vs experimental flow curves in the CE and SE.

With obstructions added in the SE, the LF approach failed to predict both static pressure and flowrate, in comparison with the experimental results, the LF witnessed a significant deviation which was calculated to be 508.33 (Pa) in the maximum generated static pressure and $8.79 \times 10^{-3}\ m^3.s^{-1}$ in the maximum delivered flowrate. However, the MRF approach succeeded in predicting flowrate with an error of 3.9% but failed to predict static pressure as it exhibited a difference of 387.99 (Pa) in the maximum generated static pressure. Fig. 13 depicts the fan performance curves derived from the experimental and numerical results.

Table 7
Experimental and CFD static pressure and flowrate readings.

Environment	Experiment	LF	MRF
FE			
Static pressure P (Pa)	428 ± 6.22	602.19	494.45
Flowrate $\dot{Q}$ $(m^3.s^{-1} \times 10^{-3})$	29.26 ±0.15	26.18	26.89
Percent error in maximum pressure (%)	-	40	15.5
Percent error in maximum flowrate (%)	-	11	8.1
CE			
Static pressure P (Pa)	238.89 ±1.33	621.55	485.74
Flowrate $\dot{Q}$ $(m^3.s^{-1} \times 10^{-3})$	28.79 ±0.14	28.22	25.67
Percent error in maximum pressure (%)	-	160	103
Percent error in maximum flowrate (%)	-	2	10.8
SE			
Static pressure P (Pa)	101.32 ±1.22	609.65	489.31
Flowrate $\dot{Q}$ $(m^3.s^{-1} \times 10^{-3})$	12.51 ±0.06	21.3	12.02
Percent error in maximum pressure (%)	-	502	388
Percent error in maximum flowrate (%)	-	70.3	3.9

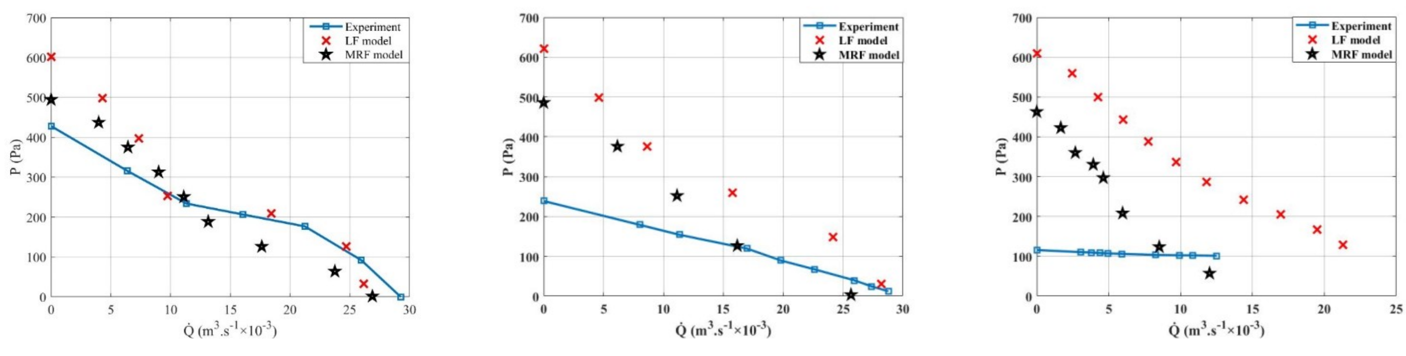

(a) FE (b) CE (c) SE

Fig. 13. Experimental and numerical fan performance curves in different environments.

As can be noted from Fig. 13, in the CE and SE environments, the fan experiences a drop in the static pressure. However, the numerical approaches estimate the static pressure in these environments without considering this static pressure drop. In the LF model, the pressure at the fan inlet is predefined using the pressure jump equation as a boundary condition. Therefore, the fan is not experiencing a considerable drop in the generated static pressure. Based on the fact that fans that can generate a higher maximum static-pressure are more capable of overcoming the flow resistance, the flow delivered by the LF model is slightly reduced when installed in condensed environments.

Regarding the MRF model, the computational domain is divided into three subdomains which are the inlet and outlet stationary zones and the fan rotating zones. At the interface between these zones, the absolute velocity values in one zone are being enforced by the CFD code to satisfy the continuity equation to calculate the velocity in the adjacent zone, while the other scalar quantities, for instance, temperature, pressure, density, and turbulent kinetic energy passed without any special treatment. This might be the reason behind the error in the MRF model pressure results. Further investigation should be conducted to uncover the reason behind the reduction in the fan static pressure when installed near a blockage in future studies. Also, this should be used to find the exact reason behind the mismatch between the MRF model results and the experimental results.

4.3. Analysis of fan flow field

Besides the fan flowrate and static pressure, the flow field created by the fan play a vital role in evaluating the fan's cooling performance. Given that fans with different flow fields will cause different temperature distributions, it is essential to study the flow field within the ITE. In the case of this study, it was done using MRF and LF. Since, MRF utilizes the actual fan body to define the flow field, while LF assumes a uniform flow field distribution, they are predicting different flow patterns. The fan flow field generated by each approach is illustrated in Fig. 14.

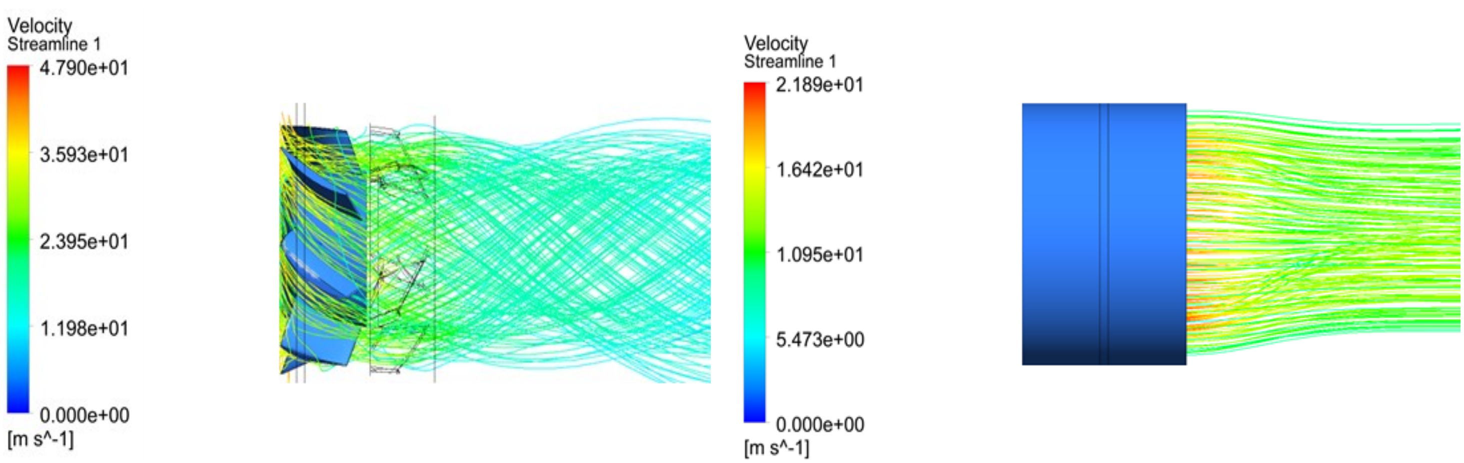

(a) MRF (b) LF

Fig. 14. Fan flow field generated by MRF and LF approaches.

The flow field created by the two modeling approaches was investigated in the three environments. Fig. 15 displays the velocity contours for cases 1–6 at the fan inlet. This figure demonstrates that the MRF and LF velocity contours at the fan inlet are completely different, which indicates that upstream of the fan the flow distribution must also be dissimilar. As a result, this will be reflected in temperature distribution inside the ITE. Moreover, Fig. 15 shows that the LF and MRF approaches react to the presence of obstructions in different ways. The velocity contours for cases 5 and 6 show how the velocity distribution changes when the server components are installed. By comparing the velocity contours for these cases, it can be inferred that the flow field of the MRF is more sensitive to blockages At the fan inlet for case 6 (MRF), the flow shows a higher velocity in the upper half of the fan, whereas for case 5 (LF) it shows near equal velocities in the upper and lower halves of the fan.

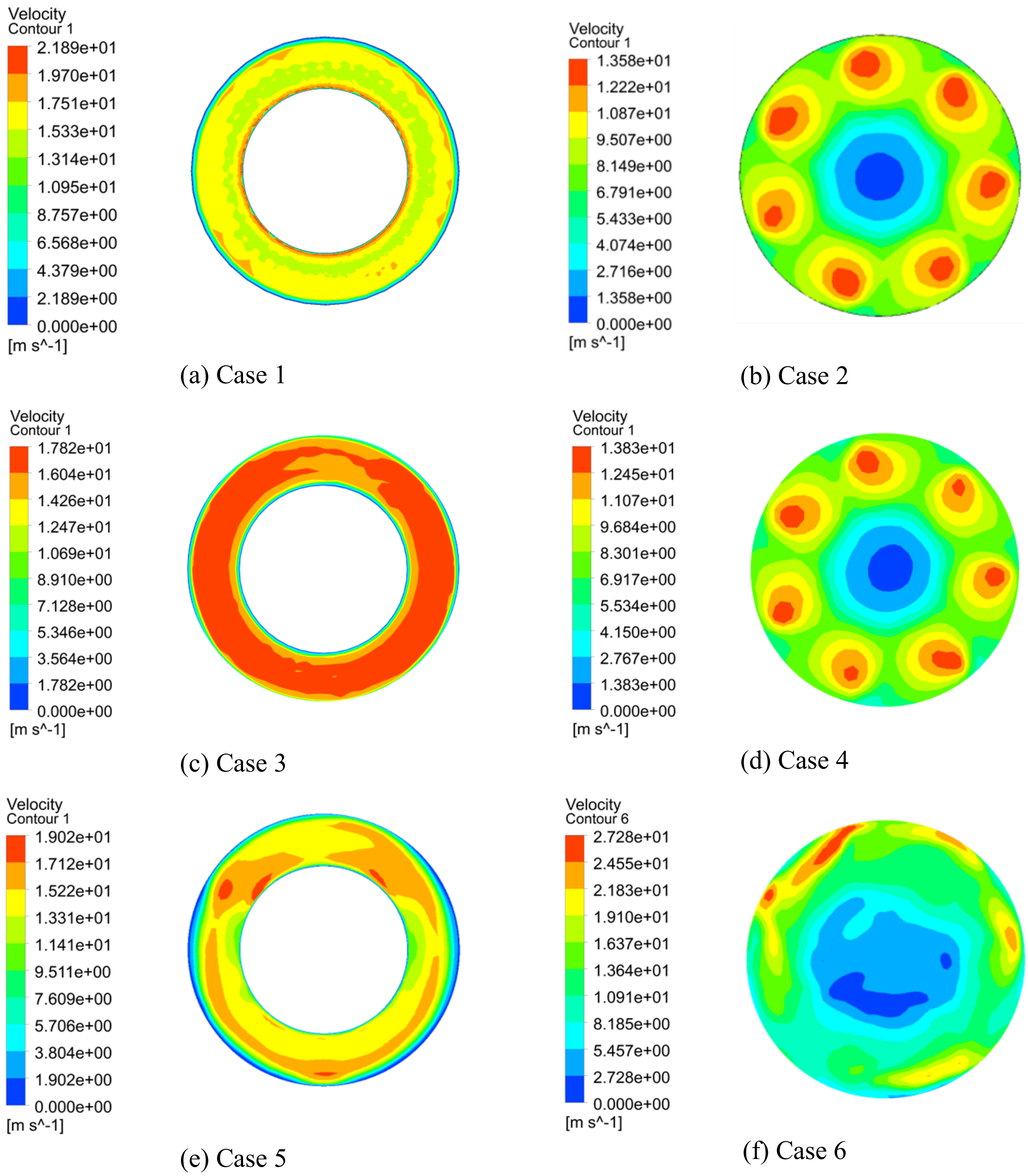

Fig. 15. Velocity contours at the fan inlet.

Further investigation was carried out for the velocity distribution at the fan outlet. Fig. 16 shows the velocity contours for cases 1–6 at the fan outlet. Much like with the velocity inlet contours, the MRF and LF models generate different velocity distributions at the fan outlet in each environment. In the MRF models, the fan outlet guide vanes were considered. By comparing the inlet velocity contours with outlet ones, it clear that the flow is more uniformly distributed at the fan inlet.

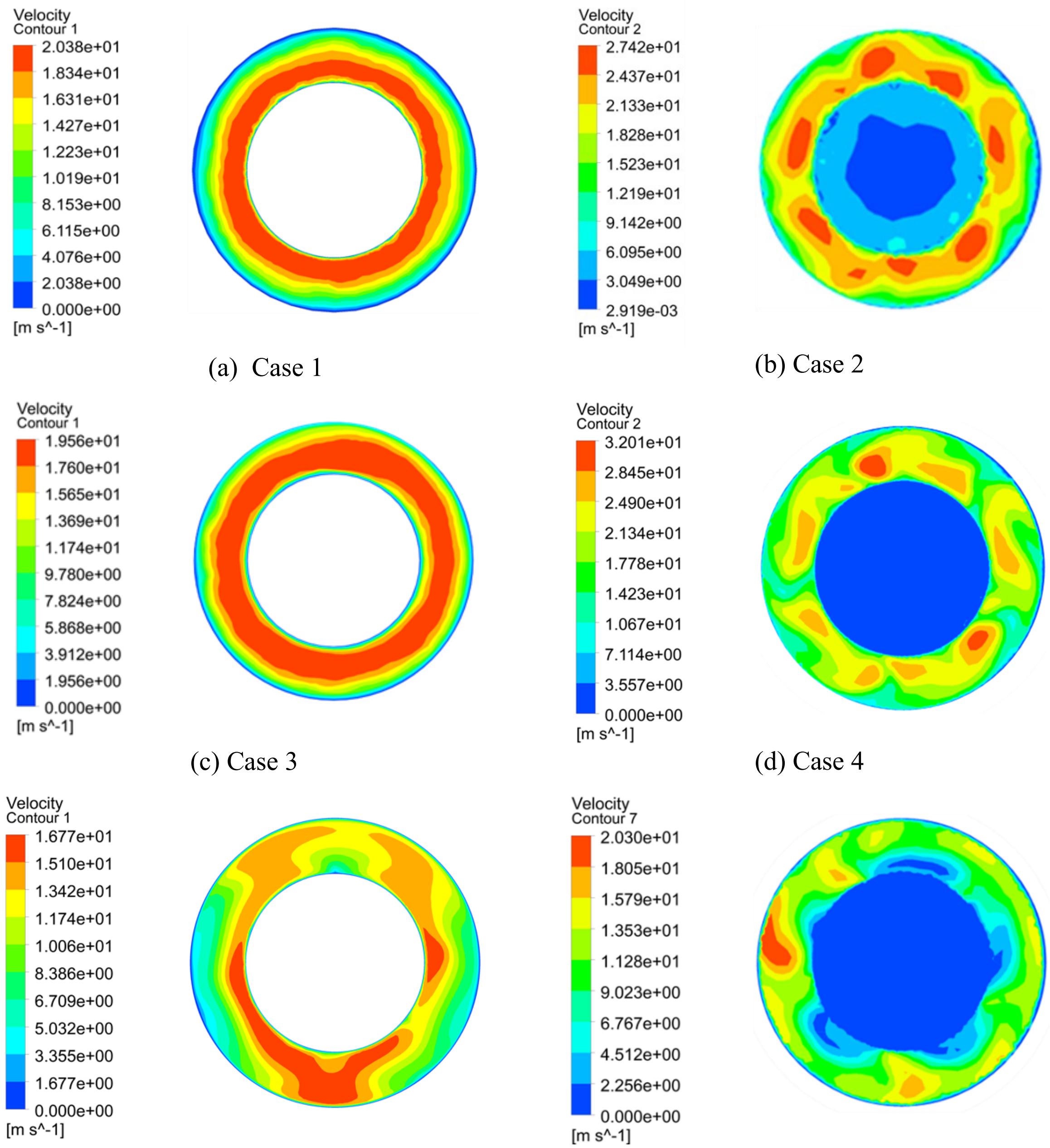

(a) Case 1 (b) Case 2

(c) Case 3 (d) Case 4

(e) Case 5 (f) Case 6

Fig. 16. Velocity contours at the fan outlet

In the LF model, the flow field is uniform at the fan inlet when no obstructions are installed as the inlet surface is assumed to have a constant pressure jump along the surface. However, due to the friction forces between the flow and fan walls, the flow profile reshapes to have a higher velocity in the middle. On the other hand, the MRF tends to have a higher velocity between the fan blades at the fan inlet, this is attributed to the fact the rotating frame is not actually rotating, instead a constant rotational speed is assigned to this frame. At the fan outlet, the flow reshapes due to the interaction with the fan's outlet guide vanes.

4.4. Analysis of the flow field inside the heat sink

Finally, to better understand how the LF and MRF approaches affect the heat transfer prediction within the ITE (cases 5 and 6), the velocity field in the heat sink was explored. The heat sink lies 16 $m \times 10^{-3}$ away from the fan outlet, as shown in Fig. 4 (e). In the LF model, the flowrate through the heat sink was calculated as 11.87 $m^3.s^{-1} \times 10^{-3}$. For the MRF model, the flowrate was equal to 7.07 $m^3.s^{-1} \times 10^{-3}$. Furthermore, the Reynolds number (Re) calculated for the LF and MRF models were found to be 385 and 228.9, respectively. Hence, the overall heat transferred from the heat sink is overpredicted in the LF model due to the higher flowrate considered and the elevated heat transfer coefficient. Fig. 17 shows the velocity contours at the corresponding heat sink.

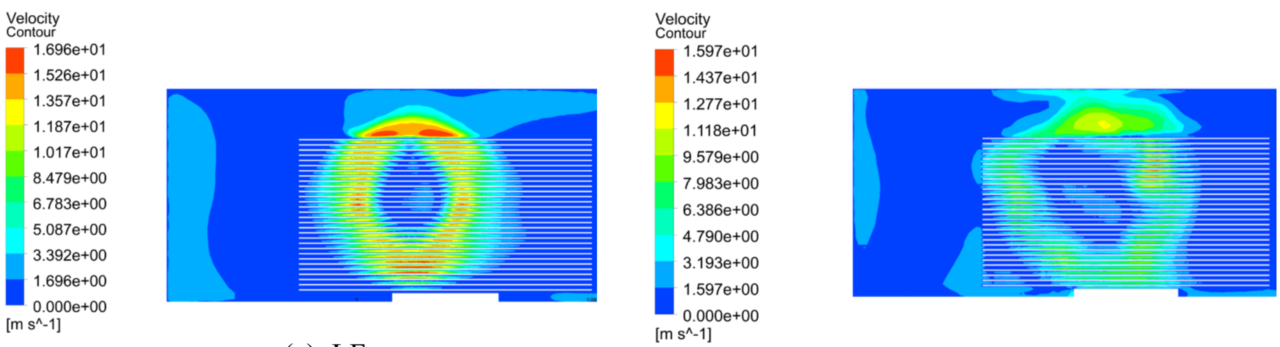

(a) LF (b) MRF

Fig. 17. Velocity contours at the inlet of the heat sink at the fan outlet.

5. Conclusions

Based on these experimental results, it can be concluded that the fans encounter a steep reduction in static pressure when they are installed in the ITE enclosure. When the ITE equipment components are considered, a huge degradation in the overall fan performance is noted. The fan flowrate and the static pressure decrease by 57.2% and 76.3%, respectively This effect of blockage on the fan performance cannot be inferred from the fan performance curve. Hence, it is extremely important to consider and investigate how the fan reacts to the presence of blockages before using it in ITE. Moreover, when testing a fan inside ITE, it is necessary to consider local pressure measurement rather than the flow test chamber to report the static pressure readings.

Comparing the numerical LF and MRF approaches with the experimental results show that both models can predict the fan performance in the FE. Inside ITE, the LF approach overestimates the flowrate delivered by the test fan by an additional 8.79 $m^3.s^{-1} \times 10^{-3}$. Moreover, the LF model static pressure is not affected by the presence of obstructions, contrasting the experimental results. The MRF model flowrate shows a good agreement with the experimental results in the three different environments with a maximum error of 10.8%. However, this approach failed to predict the fan's static pressure.

Consequently, the LF model's overestimation of flowrate results in an overvaluation of the Re and flowrate through the heat sink at the back of the fan. The flowrate and Re calculated using the LF model are 67.9% and 68.2%, respectively, which are higher than those calculated using the MRF approach.

Ultimately, the LF approach is deemed suitable for applications with no obstructions around the fan, but it is not recommended for predicting the flow field or heat transfer in highly restrictive environments. Instead, using the MRF approach in these environments could significantly decrease the error. Furthermore, when

MRF is employed in such environments no conclusions should be carried out regarding the static pressure readings.

Acknowledgments

We would like to acknowledge, Future Facilities Ltd and ES2 Partner Universities for their support and advice. Also, authors would like to acknowledge the reviewers for their constructive comments. This work is supported by NSF IUCRC Award No. IIP- 1738793 and MRI Award No. CNS1040666.

References

[1] V. Choudhari, A. Dhoble, S. Panchal, Numerical analysis of different fin structures in phase change material module for battery thermal management system and its optimization, International Journal of Heat and Mass Transfer, 163 (2020) 120434.
[2] Y. Lai, W. Wu, K. Chen, S. Wang, C. Xin, A compact and lightweight liquid-cooled thermal management solution for cylindrical lithium-ion power battery pack, International Journal of Heat and Mass Transfer, 144 (2019) 118581.
[3] D. Kong, R. Peng, P. Ping, J. Du, G. Chen, J. Wen, A novel battery thermal management system coupling with PCM and optimized controllable liquid cooling for different ambient temperatures, Energy Conversion and Management, 204 (2020) 112280.
[4] L. Zhao, Z. Zheng, B. Guo, Z. Yang, Experimental investigation on the thermal performance of air-cooled multi-port flat heat pipes, International Journal of Heat and Mass Transfer, 154 (2020) 119600.
[5] M. Bahiraei, S. Heshmatian, Electronics cooling with nanofluids: a critical review, Energy Conversion and Management, 172 (2018) 438-456.
[6] Y.M. Manaserh, M.I. Tradat, G. Mohsenian, B.G. Sammakia, M.J. Seymour, General Guidelines for Commercialization a Small-Scale In-Row Cooled Data Center: A Case Study, in: 2020 36th Semiconductor Thermal Measurement, Modeling & Management Symposium (SEMI-THERM), IEEE, 2020, pp. 48-55.
[7] C. Caceres, A. Ortega, A. Wemhoff, G.F. Jones, Numerical Analysis of Two Phase Cross-Flow Heat Exchanger for High Power Density Equipment in Data Centers under Dynamic Conditions, in: 2020 19th IEEE Intersociety Conference on Thermal and Thermomechanical Phenomena in Electronic Systems (ITherm), IEEE, 2020, pp. 520-529.
[8] C.H. Hoang, M. Tradat, Y. Manaserh, B. Ramakrisnan, S. Rangarajan, Y. Hadad, S. Schiffres, B. Sammakia, Liquid Cooling Utilizing a Hybrid Microchannel/Multi-Jet Heat Sink: A Component Level Study of Commercial Product, in: ASME 2020 International Technical Conference and Exhibition on Packaging and Integration of Electronic and Photonic Microsystems, American Society of Mechanical Engineers Digital Collection, 2020.
[9] M. Tradat, G. Mohsenian, Y. Manaserh, B. Sammakia, D. Mendo, H.A. Alissa, Experimental Analysis of Different Measurement Techniques of Server-Rack Airflow Predictions Towards Proper DC Airflow Management, in: 2020 19th IEEE Intersociety Conference on Thermal and Thermomechanical Phenomena in Electronic Systems (ITherm), IEEE, 2020, pp. 366-373.
[10] Mohammad I. Tradat, Yaman M. Manaserh. Bahgat G. Sammakia, Cong Hiep Hoang, Husam A. Alissa, An Experimental and Numerical Investigation of Novel Solution for Energy Management Enhancement in Data Centers Using Underfloor Plenum Porous Obstructions. Applied Energy, In press (Accepted) (2021).

[11] A. Taheri, M.G. Moghadam, M. Mohammadi, M. Passandideh-Fard, M. Sardarabadi, A new design of liquid-cooled heat sink by altering the heat sink heat pipe application: Experimental approach and prediction via artificial neural network, Energy Conversion and Management, 206 (2020) 112485.
[12] B. Kanargi, P.S. Lee, C. Yap, A numerical and experimental investigation of heat transfer and fluid flow characteristics of an air-cooled oblique-finned heat sink, International Journal of Heat and Mass Transfer, 116 (2018) 393-416.

[13] H.H. Saber, S.A. AlShehri, W. Maref, Performance optimization of cascaded and non-cascaded thermoelectric devices for cooling computer chips, Energy Conversion and Management, 191 (2019) 174-192.
[14] T. Yeom, L. Huang, M. Zhang, T. Simon, T. Cui, Heat transfer enhancement of air-cooled heat sink channel using a piezoelectric synthetic jet array, International Journal of Heat and Mass Transfer, 143 (2019) 118484.
[15] M. Yang, M.-T. Li, Y.-C. Hua, W. Wang, B.-Y. Cao, Experimental study on single-phase hybrid microchannel cooling using HFE-7100 for liquid-cooled chips, International Journal of Heat and Mass Transfer, 160 (2020) 120230.
[16] J. Stafford, E. Walsh, V. Egan, R. Grimes, Flat plate heat transfer with impinging axial fan flows, International Journal of Heat and Mass Transfer, 53(25-26) (2010) 5629-5638.
[17] J. Stafford, E. Walsh, V. Egan, Local heat transfer performance and exit flow characteristics of a miniature axial fan, International journal of heat and fluid flow, 31(5) (2010) 952-960.
[18] D. Jang, K.-S. Lee, Flow characteristics of dual piezoelectric cooling jets for cooling applications in ultra-slim electronics, International Journal of Heat and Mass Transfer, 79 (2014) 201-211.
[19] W.L. Staats, J. Brisson, Active heat transfer enhancement in air cooled heat sinks using integrated centrifugal fans, International Journal of Heat and Mass Transfer, 82 (2015) 189-205.
[20] J. Stafford, E. Walsh, V. Egan, The effect of global cross flows on the flow field and local heat transfer performance of miniature centrifugal fans, International journal of heat and mass transfer, 55(7-8) (2012) 1970-1985.
[21] S.-C. Lin, C.-A. Chou, Blockage effect of axial-flow fans applied on heat sink assembly, Applied thermal engineering, 24(16) (2004) 2375-2389.
[22] S.-C. Lin, F.-S. Chuang, C.-A. Chou, C.-W. Sun, Z.-H. Yang, Blockage Effect of the Centrifugal Cooling Fans, in: Thermal Sciences 2004. Proceedings of the ASME-ZSIS International Thermal Science Seminar II, Begel House Inc., 2004.
[23] S. Nakamura, M. Takahashi, K. Sato, K. Yokota, Influence of an Upstream Obstacle on the Flow Characteristics of Axial-flow Fans, in: Fluids Engineering Division Summer Meeting, American Society of Mechanical Engineers, 2014, pp. V01BT10A017.
[24] K. Ochiai, S. Nakamura, K. Sato, D. Kang, K. Yokota, Flow Characteristics of Axial-Flow Fans With an Upstream/Downstream Blockage Disk, in: Fluids Engineering Division Summer Meeting, American Society of Mechanical Engineers, 2017, pp. V01AT03A011.
[25] A. Al-Salaymeh, O. Badran, The Influence of Inlet and Outlet Grilles on the Flow Characteristics of Axial Fans.
[26] T. Fukue, M. Ishizuka, T. Hatakeyama, S. Nakagawa, K. Koizumi, Study on PQ curves of cooling fans for thermal design of electronic equipment (Effects of opening position of obstructions near a fan), in: Fluids Engineering Division Summer Meeting, 2011, pp. 737-745.
[27] T. Fukue, T. Hatakeyama, M. Ishizuka, K. Hirose, K. Koizumi, Relationships between supply flow rate of small cooling fans and pressure drop characteristics in electronic enclosure, in: International Electronic Packaging Technical Conference and Exhibition, American Society of Mechanical Engineers, 2013, pp. V002T008A020.
[28] T. Fukue, K. Hirose, T. Hatakeyama, M. Ishizuka, K. Koizumi, Evaluation of pressure drop characteristics around axial cooling fans with electrical components, in: 2016 International Conference on Electronics Packaging (ICEP), IEEE, 2016, pp. 173-178.
[29] G.V. Shankaran, M.B. Dogruoz, Validation of an advanced fan model with multiple reference frame approach, in: 2010 12th IEEE intersociety conference on thermal and thermomechanical phenomena in electronic systems, IEEE, 2010, pp. 1-9.
[30] R. Boukhanouf, A. Haddad, A CFD analysis of an electronics cooling enclosure for application in telecommunication systems, Applied Thermal Engineering, 30(16) (2010) 2426-2434.
[31] P.S. Nasirabadi, S.M. Ghiaasiaan, J.H. Hattel, Long term prediction of local climate inside an electronics enclosure, International Journal of Heat and Mass Transfer, 137 (2019) 280-291.

[32] Z. Song, Studying the fan-assisted cooling using the Taguchi approach in open and closed data centers, International Journal of Heat and Mass Transfer, 111 (2017) 593-601.
[33] H.A. Alissa, K. Nemati, U.L. Puvvadi, B.G. Sammakia, K. Schneebeli, M. Seymour, T. Gregory, Analysis of airflow imbalances in an open compute high density storage data center, Applied Thermal Engineering, 108 (2016) 937-950.
[34] M.B. Dogruoz, G. Shankaran, Computations with the multiple reference frame technique: Flow and temperature fields downstream of an axial fan, Numerical Heat Transfer, Part A: Applications, 71(5) (2017) 488-510.
[35] J. Luo, A. Gosman, Prediction of impeller-induced flow in mixing vessels using multiple frames of reference, in, INSTITUTE OF CHEMICAL ENGINEERS SYMPOSIUM SERIES, 1994.
[36] Y.T.a.L. Lee, H.C., 2016. Performance assessment of various fan ribs inside a centrifugal blower. Energy, 94, pp.609-622.
[37] X. Ye, Zhang, J. and Li, C., 2017. Effect of blade tip pattern on performance of a twin-stage variable-pitch axial fan. Energy, 126, pp.535-563.
[38] L. Zhang, He, R., Wang, X., Zhang, Q. and Wang, S., 2019. Study on static and dynamic characteristics of an axial fan with abnormal blade under rotating stall conditions. Energy, 170, pp.305-325.
[39] B. Jiang, Wang, J., Yang, X., Wang, W. and Ding, Y., 2019. Tonal noise reduction by unevenly spaced blades in a forward-curved-blades centrifugal fan. Applied Acoustics, 146, pp.172-183.
[40] G. Shankaran, M.B. Dogruoz, Advances in fan modeling: Using multiple reference frame (mrf) approach on blowers, in: International Electronic Packaging Technical Conference and Exhibition, 2011, pp. 259-267.
[41] M.B. Dogruoz, G. Shankaran, Advances in fan modeling: issues and effects on thermal design of electronics, in: ASME International Mechanical Engineering Congress and Exposition, American Society of Mechanical Engineers, 2012, pp. 1515-1522.
[42] C. Zhou, C. Yang, C. Wang, X. Zhang, Numerical simulation on a thermal management system for a small data center, International Journal of Heat and Mass Transfer, 124 (2018) 677-692.
[43] A.A.S.-A.S. 51-16, Laboratory Methods of Testing Fans for Certified Aerodynamic Performance Rating, in, Air Movement and Control Association International Inc., 2016.
[44] K.A. Banaszynski, Design and qualification of an experimental facility for performing fluid mechanics and heat transfer measurements in a turbulent channel flow over a two-dimensional obstacle, (1992).
[45] A.A.S.-A.A. 51-1999), Laboratory method of testing fans for aerodynamic performance rating, in, Air Movement and Control Association, Inc., 1999.
[46] R.W. Whitesides, Basic Pump Parameters and the Affinity Laws, PDH Center, Fairfax, VA, (2012).
[47] R. Franzke, CFD modelling of axial fans for thermal management applications, Chalmers Tekniska Hogskola (Sweden), 2019.
[48] P. Gullberg, L. Löfdahl, S. Adelman, P. Nilsson, An Investigation and correction method of stationary fan CFD MRF simulations, 0148-7191, SAE Technical Paper, 2009.
[49] A. Kasaeian, A.R. Mahmoudi, F.R. Astaraei, A. Hejab, 3D simulation of solar chimney power plant considering turbine blades, Energy Conversion and Management, 147 (2017) 55-65.
[50] Y.-J. Jung, H. Jeon, Y. Jung, K.-J. Lee, M. Choi, Effects of recessed blade tips on stall margin in a transonic axial compressor, Aerospace Science and Technology, 54 (2016) 41-48.
[51] F. Kameier, W. Neise, Experimental study of tip clearance losses and noise in axial turbomachines and their reduction, (1997).
[52] R. Achouri, I. Mokni, H. Mhiri, P. Bournot, A 3D CFD simulation of a self inducing Pitched Blade Turbine Downflow, Energy conversion and management, 64 (2012) 633-641.
[53] H. Zhao, C. Kang, K. Ding, Y. Zhang, B. Li, Transient startup characteristics of a drag-type hydrokinetic turbine rotor, Energy Conversion and Management, 223 (2020) 113287.

[54] Z. Xu, Y.-H. Feng, C.-Y. Zhao, Y.-L. Huo, S. Li, X.-J. Hu, Y.-J. Zhong, Experimental and numerical investigation on aerodynamic performance of a novel disc-shaped wind rotor for the small-scale wind turbine, Energy Conversion and Management, 175 (2018) 173-191.
[55] M. Mohamed, Performance investigation of H-rotor Darrieus turbine with new airfoil shapes, Energy, 47(1) (2012) 522-530.
[56] A.T. Shirazi, M.R. Nazari, M.D. Manshadi, Numerical and experimental investigation of the fluid flow on a full-scale pump jet thruster, Ocean Engineering, 182 (2019) 527-539.
[57] P. Huang, P. Bradshaw, T. Coakley, Skin friction and velocity profile family for compressible turbulentboundary layers, AIAA journal, 31(9) (1993) 1600-1604.
[58] M. Peric, S. Ferguson, The advantage of polyhedral meshes, Dynamics, 24 (2005) 45.
[59] M. Spiegel, T. Redel, Y.J. Zhang, T. Struffert, J. Hornegger, R.G. Grossman, A. Doerfler, C. Karmonik, Tetrahedral vs. polyhedral mesh size evaluation on flow velocity and wall shear stress for cerebral hemodynamic simulation, Computer methods in biomechanics and biomedical engineering, 14(01) (2011) 9-22.
[60] E. Tannoury, S. Khelladi, B. Demory, M. Henner, F. Bakir, Influence of blade compactness and segmentation strategy on tonal noise prediction of an automotive engine cooling fan, Applied acoustics, 74(5) (2013) 782-787.
[61] M. Darvish, S. Frank, Numerical Investigations on the Performance Characteristic of Radial Fans with forward curved blades by means of CFD, Master Thesis, HTW Berlin, 2010.
[62] O. Singh, R. Khilwani, T. Sreenivasulu, M. Kannan, Parametric study of centrifugal fan performance: experiments and numerical simulation, International Journal of Advances in Engineering & Technology, 1(2) (2011) 33-50.
[63] X. Ye, X. Ding, J. Zhang, C. Li, Numerical simulation of pressure pulsation and transient flow field in an axial flow fan, Energy, 129 (2017) 185-200.
[64] M. Stevens, Fan performance, Air Movement and Control Association International, (2016).
[65] L. Twin City Fan Companies, Fan Engineering: Temperature & Altitude Effects On Fans, 2018.